Optical Materials 131 (2022) 112613

Contents lists available at ScienceDirect

Optical Materials

journal homepage: www.elsevier.com/locate/optmat

Research Article

Bright white light up-conversion luminescence from $Yb^{3+}/Er^{3+}/Tm^{3+}$ tridoped gadolinium gallium garnet nano-crystals for multicolor and white light-emitting diodes

Hümeyra Örücü [a,*], Sevcan Tabanli [b], Murat Erdem [c], Yavuz Öztürk [d], Gönül Eryürek [b]

[a] Ege University, Physics Department, 35040, Izmir, Turkey
[b] Istanbul Technical University, Physics Engineering Department, 34469, Istanbul, Turkey
[c] Marmara University, Physics Department, 34777, Istanbul, Turkey
[d] Ege University, Electric Electronic Engineering Department, 35040, Izmir, Turkey

ARTICLE INFO

Keywords:
Nanophosphors
Gadolinium gallium garnet (GGG)
Up-conversion
Color chromaticity coordinates
WLED

ABSTRACT

Gadolinium Gallium Garnet nanophosphors with $Yb^{3+}/Er^{3+}/Tm^{3+}$ triply-doped ions were synthesized via the Solgel Pechini method and annealed at different temperatures ranging from 800 to 1200 °C. The approximate average crystallite sizes were determined within the range of 26–56 nm by using X-ray diffraction analysis. Color-tunable up-conversion emission was explored in nanomaterials by varying excitation power under 975 nm excitation wavelength by varying excitation power and Tm^{3+} concentration for white light emission. Bright white light up-conversion luminescence from $Yb^{3+}/Er^{3+}/Tm^{3+}$ tridoped $Gd_3Ga_5O_{12}$ was recorded. The color quality coordinates for $Gd_3Ga_5O_{12}$:2%Yb^{3+}/1%Er^{3+}/1.5%Tm^{3+} nanophosphors annealed at 1000 °C were found to be x = 0.3244, y = 0.3297 at room temperature under 975 nm infrared excitation, which falls within the white zone of the 1931 International Commission on Illumination diagram. Nanophosphors show extreme near-infrared radiation at 800 nm, which is also beneficial to deeper tissue penetration and promotes plants' growth.

1. Introduction

Rare earth (RE) activated up-conversion nanophosphors (UCNPs), which generates visible light under near-infrared excitation, have attracted considerable interest since they find potential applications in fluorescent biological imaging, solid-state lighting, displays, the back-light of LCD screens, optical thermometric materials, and white light-emitting diodes (WLEDs) [1–3]. Particularly, phosphor-converted WLEDs (pc-WLEDs) use a diode that pumps a single or combination of phosphors. The performance and quality of the WLEDs are affected by the luminescence properties of the phosphors.

There is growing demand for new and efficient RGB-based (red, green, blue) white-light emission nanophosphors, which can serve as lightning sources over the conventional incandescent and fluorescent lamps for solid-state lighting and indoor plant growing [4–6]. Therefore, more and more attention has been paid to the development of single-component white light-emitting nanophosphors with single, co-doped, or tridoped rare-earth ions to improve the color properties of the WLED devices.

Rare-earth ions activated garnets are promising hosts for white light generation studies owing to physical, chemical, and optical properties such as hardness, high thermal stability, optical isotropy, thermal conductivity and possess some advantages due to two or more RE^{+} centers for the generation of multicolor emission [7–12]. Gadolinium gallium garnet ($Gd_3Ga_5O_{12}$, GGG) nanocrystals are a promising host material for up-conversion (UC) emission with a higher melting point (~1740 °C), higher refractive index (~2), and lower phonon energy (~650 cm^{-1}) [13,14].

Up to now, there have been several reports on up-conversion luminescence from single-doped (Er^{3+}, Nd^{3+}, Eu^{3+}) [15–20] and co-doped (Eu^{3+}-Yb^{3+}, Nd^{3+}-Yb^{3+}, Ho^{3+}-Yb^{3+}, Er^{3+}-Yb^{3+}, Pr^{3+}-Yb^{3+}, Tm^{3+}-Yb^{3+}) [2,19–24] nano-crystalline gadolinium gallium garnets.

Our group has recently reported for the first time the fabrication of Yb^{3+}/Er^{3+} co-doped GGG nanophosphors that display bright white, and green up-conversion luminescence preliminarily explored a possibility for optical thermometry [24].

However, to the best of our knowledge, little research has reported on the UC-photoluminescence properties of tridoped (Yb^{3+}/Tm^{3+}/

* Corresponding author.
E-mail address: humeyra.orucu@ege.edu.tr (H. Örücü).

https://doi.org/10.1016/j.optmat.2022.112613
Received 10 March 2022; Received in revised form 10 June 2022; Accepted 12 June 2022
Available online 22 June 2022

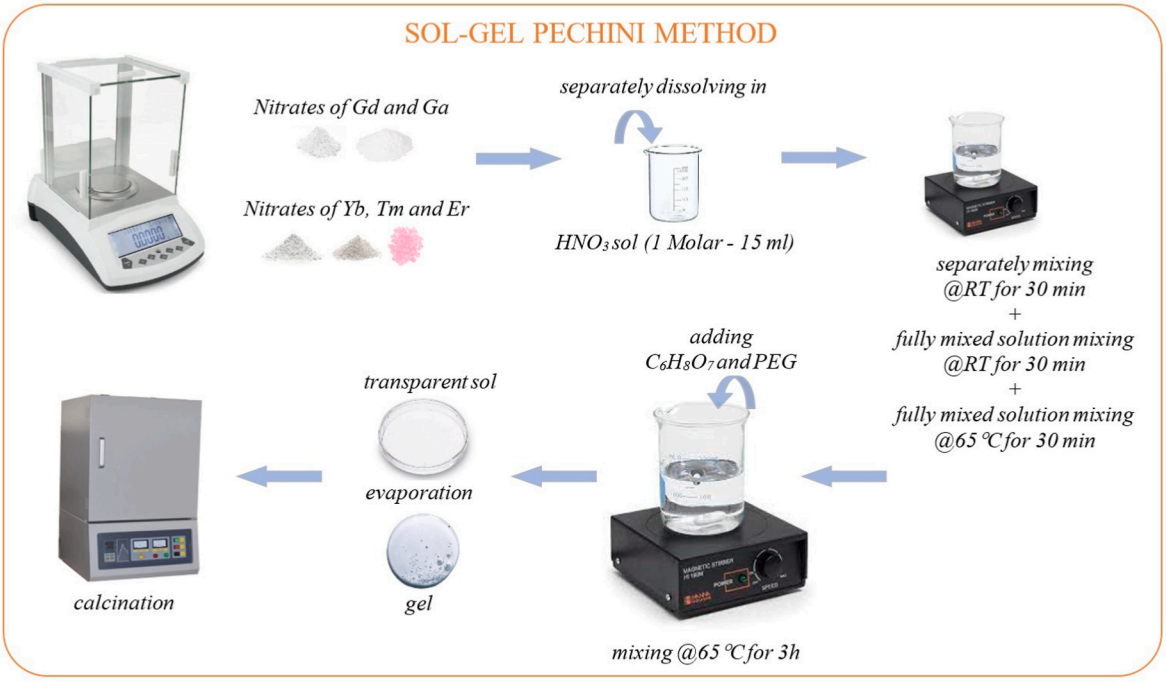

Fig. 1. Synthesis Procedure of the $Yb^{3+}/Er^{3+}/Tm^{3+}$: GGG Nanophosphors.

Ho^{3+}, $Ce^{3+}/Tb^{3+}/Yb^{3+}$, $Yb^{3+}/Bi^{3+}/Er^{3+}$, $Yb^{3+}/Er^{3+}/Tm^{3+}$) $Gd_3Ga_5O_{12}$ phosphors [25–29]. Two studies have been carried out in the literature on $Yb^{3+}/Er^{3+}/Tm^{3+}$ triply doped GGG-based white light studies. Firstly, Mahalingam et al. studied the up-conversion emission properties of Yb^{3+}(10 mol%)/Er^{3+}(1 mol %)/Tm^{3+}(1 mol %): $Gd_3Ga_5O_{12}$ prepared via Pechini method [29]. The nanocrystalline GGG sample did not produce white light and hardly any light was observed.

Secondly, Sun et al. investigated the up-conversion emission properties of Yb^{3+}(x mol%)/Er^{3+}(1 mol %)/Tm^{3+}(1 mol %): $Gd_3Ga_5O_{12}$ (x mol % = 1, 3, 5, 10) prepared via a simple citric acid propellant combustion method [28]. As a result, their XRD patterns of $Gd_3Ga_5O_{12}$ indicate the cubic $Gd_3Ga_5O_{12}$, Ga_2O_9, and Gd_2O_3 phases. A white UC emission was achieved for Yb^{3+}(10 mol%)/Er^{3+}(1 mol %)/Tm^{3+}(1 mol %): $Gd_3Ga_5O_{12}$ nanocrystals under 974.5 nm laser excitation. It is shown that multicolor rare-earth-doped UC-emission depends on phosphor synthesis methods, the concentration of the doping ions, activators/sensitizers, size symmetry, and excitation laser power.

In this work, to obtain multicolor and white emission in visible region $Yb^{3+}/Er^{3+}/Tm^{3+}$ tridoped GGG phosphors with various dopant ratios were prepared via Solgel Pechini method by using polyethylene glycol as a cross-linking agent and citric and nitric acid as a chelating agent. Their optical behaviors are studied by the 975 nm excitation power of the laser diode as the excitation source.

2. Experimental methods

2.1. Material synthesis

A series of $Yb^{3+}/Er^{3+}/Tm^{3+}$ tridoped $Gd_3Ga_5O_{12}$ powder phosphors were prepared using the Solgel Pechini method with nitrates of Ga, Gd, Yb, Er, Tm and then annealed at 800, 1000, and 1200 °C for 2 h. Gd $(NO_3)_3.6H_2O$ (99.99%), $Ga(NO_3)_3.H_2O$ (99.99%), $Yb(NO_3)_3{\cdot}5H_2O$ (99.9%), $Er(NO_3)_3.5H_2O$ (99.99%), and $Tm(NO_3)_3.5H_2O$ (99.99%) were used as starting materials. All materials were purchased from Sigma-Aldrich company. The rare-earth ions dopant ratios for the GGG powders are 2.0 mol% Yb^{3+}, 1.0 mol% Er^{3+} and *x* mol% Tm^{3+} ($x = 0.5$, 1.0, 1.5 and labeled as GGG:YET1, GGG:YET2, and GGG:YET3, respectively). The further synthesis procedure of the nanophosphors is summarized in Ref. [24]. Briefly, all starting materials were weighted at stoichiometric ratios (Gd/Ga = 0.56) based on (1 M) was added to the solution under fixed stirring to dissolve the materials. Citric acid as a chelate ligand and polyethylene glycol (PEG) as a cross-linking agent were added under constant stirring at 65 °C for 3 h to obtain the highly transparent gel (Fig. 1). After the transparent sols were obtained, they aged for ten days at room temperature. Then the samples precursors were annealed in the muffle furnace at 800, 1000, and 1200 °C at a 7 °C/min^{-1} heating rate for 2 h.

2.2. Characterization

The crystal structures of the tridoped gadolinium gallium garnet phosphors were examined using the X-ray diffraction (XRD) technique. The XRD spectra were taken using Rigaku–XRD diffractometer (2200 D/MAX, Japan), operating at 40 kV source voltage and 30 mA between 10° and 70° (2θ) under Cu-Kα radiation (λ = 0.15418 nm). Crystalline phases were identified by comparison with the Joint Committee on Powder Diffraction Standards (JCPDS) database.

Diffusive reflectance spectra were taken to identify the absorption lines of RE^{3+} ions in GGG nanophosphors. A PerkinElmer Model Lambda 35 UV–Vis spectrometer was used to record the diffusive reflectance spectra in the range of 400–1000 nm at room temperature.

The up-conversion emission spectra of the nanopowders were obtained in the range of 400–850 nm during the excitation of a 975 nm laser diode (CNI MDL-H-975 Model). The emission from the nanophosphors was focused on a monochromator (Princeton Inst.-SP2500i) and detected by an Acton series-SI440 silicon detector. A short pass filter was placed in front of the monochromator slit (Edmund optics, 950 nm) to block the scattered excitation light. The laser pump power was determined using a power meter (Coherent Field Max II-TOP Model).

AsenseTek-Lighting Passport Model Illuminance Meter was used to determine the color quality parameters such as the color chromaticity coordinates (CIE-1931), the color rendering index (CRI), and the correlated color temperature (CCT). All the measurements were recorded at room temperature.

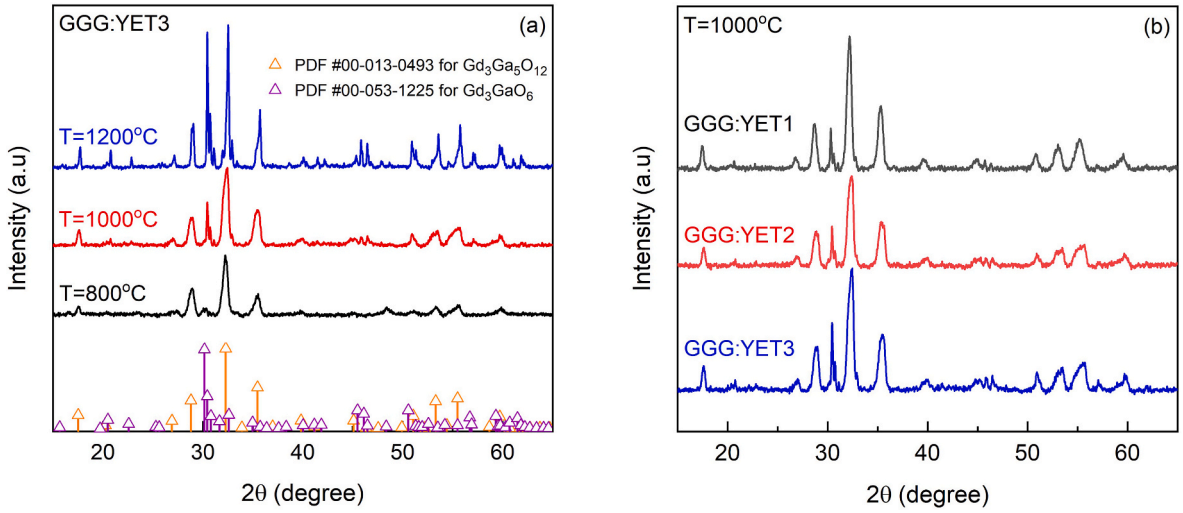

Fig. 2. XRD patterns of the GGG:YET3 nanophosphors annealed at different temperatures (a), and GGG nanophoshors with different Yb/Er/Tm doping concentrations (b).

Table 1
Average crystallite sizes of GGG: YET nanophosphors.

Samples ID	T = 800 °C	T = 1000 °C	T = 1200 °C
GGG: YET1	26	29	51
GGG: YET2	28	31	50
GGG: YET3	28	30	56

3. Results and discussion

3.1. Structural properties

The X-ray diffraction spectra of the GGG:Yb^{3+}/Er^{3+}/Tm^{3+} nanocrystals were investigated to confirm the phase purity of the nanophosphors (Fig. 2). The crystalline single-phase structure of cubic $Gd_3Ga_5O_{12}$ (garnet) phase (JCPDS card no 53–1225) is identified for powders heat-treated at 800 °C. A small amount of secondary orthorhombic Gd_3GaO_6 (gallate) phase (JCPDS card no 13–0493) slowly grows as annealing temperature increases. $Gd_3Ga_5O_{12}$ (garnet) phase has been stayed dominant for all samples annealed at different temperatures. In addition, the proportions of areas under the most intense peak corresponding to the two phases, can provide a relative evaluation for all nanocrystals. It is observed in Fig. 2, as the concentration increases, the content ratio corresponding to the relative area ratios in favor of the garnet phase increases. The ionic radius of the Yb^{3+} and Tm^{3+} ion [30] is smaller than the ionic radius of the Er^{3+} ion. It has been suggested that the gallate phase will not occur for rare earth elements with an ionic radius greater than Nd^{3+} and less than Er^{3+} ion [31]. Therefore, we can say that Yb^{3+} and Tm^{3+} ions mostly prefer to replace Gd^{3+} ions in the garnet phase compared to the gallate phase.

XRD spectra of the samples labeled as GGG:YET3 with different annealing temperatures are given in Fig. 2(a) as an example. The diffraction peaks indicate that the crystal lattice structure of the host is not affected by the RE^{3+} dopant ions. The XRD patterns of GGG nanophosphors with different Yb^{3+}/Er^{3+}/Tm^{3+} doping concentrations are shown in Fig. 2(b). The main peaks (2θ = 32.3°) gently shifted to the larger angles with the rise of RE^{3+} ion concentration, caused by the discrepant ionic radii between the Gd^{3+} (1.053 Å; the coordinate number is 8) and RE^{3+} (Yb^{3+}: 0.99 Å, Tm^{3+}: 0.99 Å, and Er^{3+}: 1.00 Å for the eight coordinate numbers) ions [30,31].

The average crystallite size (D) was calculated by the Scherrer equation [32], $D = K\lambda/\beta cos\theta$, where K is the dimensionless shape factor, has a value of about 0.9, λ is the X-ray wavelength (0.15418 nm), β is the full-width at half maximum (FWHM) of the peak, and θ is the diffraction angle. The most substantial peak at $2\theta = 32.29°$ was chosen to analyze the crystallite sizes of the powder samples. The particle size of the

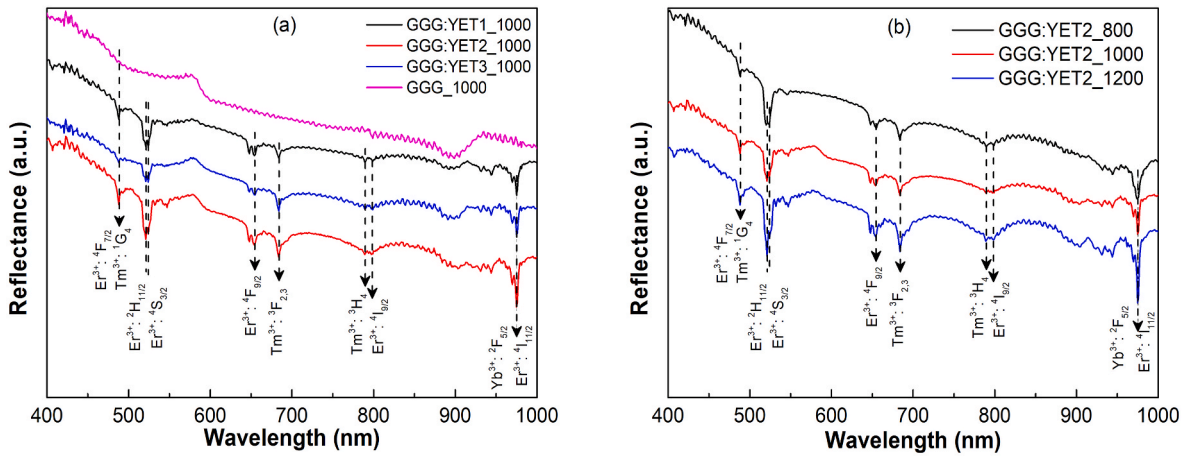

Fig. 3. Reflectance spectra of GGG:Yb^{3+}/Er^{3+}/Tm^{3+} nanocrystals and undoped GGG samples with 1000 °C annealing temperature (a), GGG:YET2 nanopowder with different annealing temperatures (b).

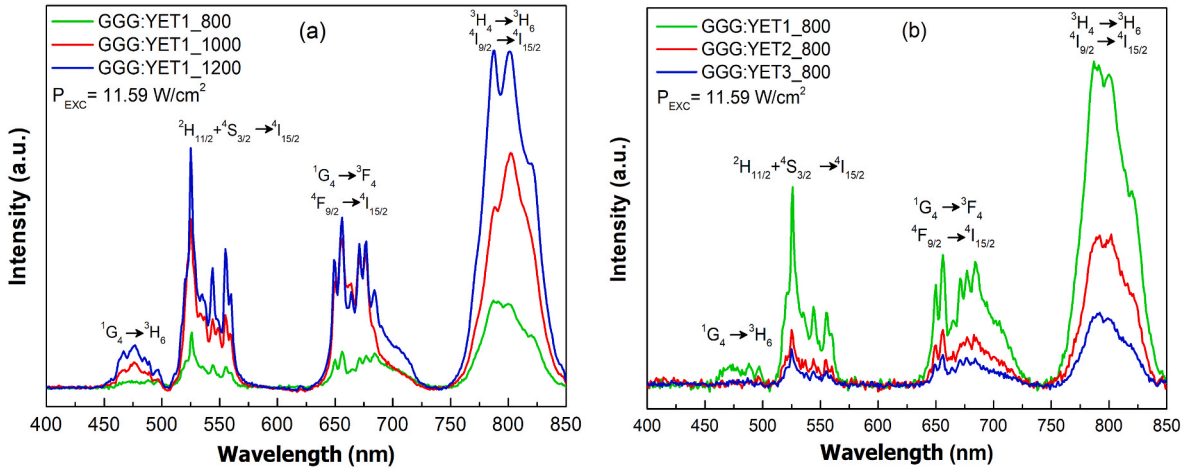

Fig. 4. Annealing temperature effect on the UC-emission spectra of the GGG: YET1 nanopowders (a). UC-emission spectra of GGG:2.0%Yb^{3+}/1.0%Er^{3+}/x%Tm^{3+} (x = 0.5, 1, 1.5) annealed at 800 °C (b).

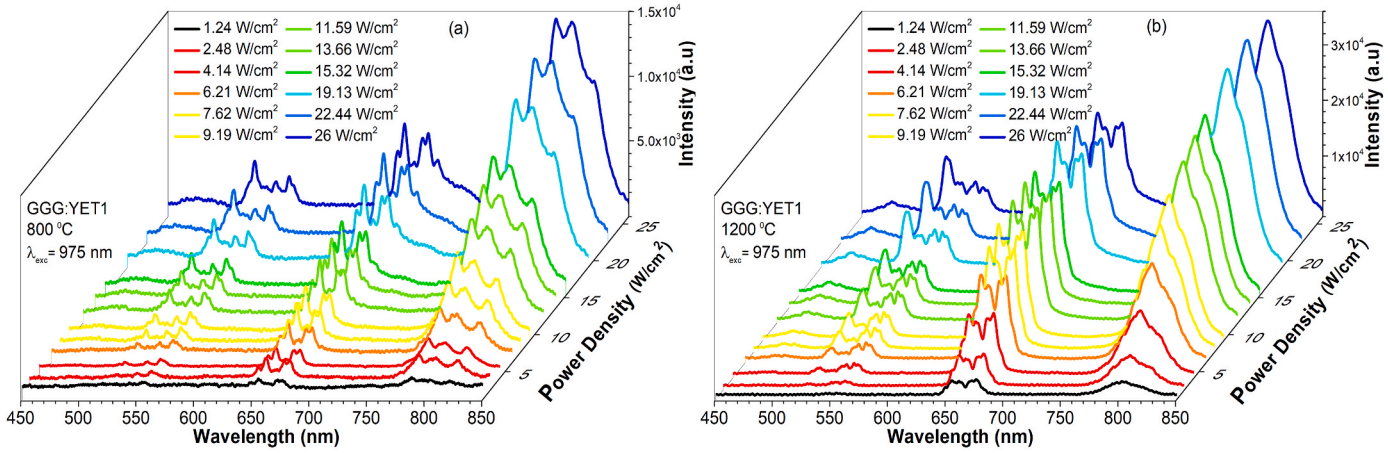

Fig. 5. Effect of the laser excitation power on the photoluminescence spectra of the GGG: YET1 nanophosphors annealed at (a) 800 °C and (b) 1200 °C.

nanopowders is listed in Table 1. The results indicate that the particle sizes increase with increasing annealing temperature.

3.2. Diffuse reflectance measurements

Fig. 3 gives the diffusive reflectance spectra of GGG:Yb^{3+}/Er^{3+}/Tm^{3+} nanophosphors and undoped GGG nanocrystal samples. To compare the effect of both the dopant concentration and the heat treatment on the profile and the peak positions of the transitions, reflectance spectra of GGG:Yb^{3+}/Er^{3+}/Tm^{3+} nanocrystals, undoped GGG samples with 1000 °C annealing temperature and GGG:YET2 nanopowder with different annealing temperatures were given in Fig. 3 (a) and (b), respectively. The profile and the peak position of each transition remain almost same with changing dopant concentration and heat treatment suggesting that there is no appreciable change in the structure of the nanoophosphors for the local environment of the dopant.

3.3. Up-conversion emission properties

Fig. 4 illustrates the UC-emission spectra of Yb^{3+}/Er^{3+}/Tm^{3+} triply doped GGG in the 400–850 nm wavelength region under 975 nm excitation with the diode laser. The influence of annealing temperature and Tm^{3+} doping content on the RGB emission intensity were given in Fig. 4 (a) and (b), respectively. Each spectrum consists of four bands corresponding to blue, green, red, and near-infrared (NIR) emissions. The blue emission corresponding to the $^1G_4 \rightarrow {}^3H_6$ transition of Tm^{3+} ion is approximately 476 nm. The $^2H_{11/2} \rightarrow {}^4I_{15/2}$ and $^4S_{3/2} \rightarrow {}^4I_{15/2}$ transitions of Er^{3+} ions are centered at about 525 and 547 nm and correspond to the green emissions. The red emissions around 673 and 655 nm correspond to the $^4F_{9/2} \rightarrow {}^4I_{15/2}$ and $^1G_4 \rightarrow {}^3F_4$ transitions of Er^{3+} and Tm^{3+} ions, respectively. The NIR emissions correspond to the $^4I_{9/2} \rightarrow {}^4I_{15/2}$ and $^3H_4 \rightarrow {}^3H_6$ transitions of Er^{3+} and Tm^{3+} ions, respectively.

The annealing temperature dependency of the emission intensity for GGG:YET1 is depicted in Fig. 4(a). UC-emission intensities increase with the increasing annealing temperatures. Fig. 4(b) indicates that as the Tm^{3+} concentration increases, UC-emission intensities decrease. The number of irradiated nanoparticles per unit volume increases with the increasing content of Tm^{3+} ions, the average distance between Tm^{3+} ions decreases, the energy transfer possibility increases and leads to the decrease in up-conversion luminescence intensity [33,34].

The UC-photoluminescence spectra of nanocrystal phosphors were also measured in the range of 400–850 nm under 975 nm excitation with the diode laser by varying the excitation power between 1.24 W/cm^2 and 26 W/cm^2. Fig. 5 shows the UC spectra of GGG: YET1 nanopowders at lower and higher annealing temperatures. The emission peaks of the Yb^{3+}/Er^{3+}/Tm^{3+} tridoped powders have blue, green, red, and NIR emissions, as shown in Fig. 5. The up-conversion emission of nanophosphors increases with the increasing excitation power and shows a decrease after saturation reaching.

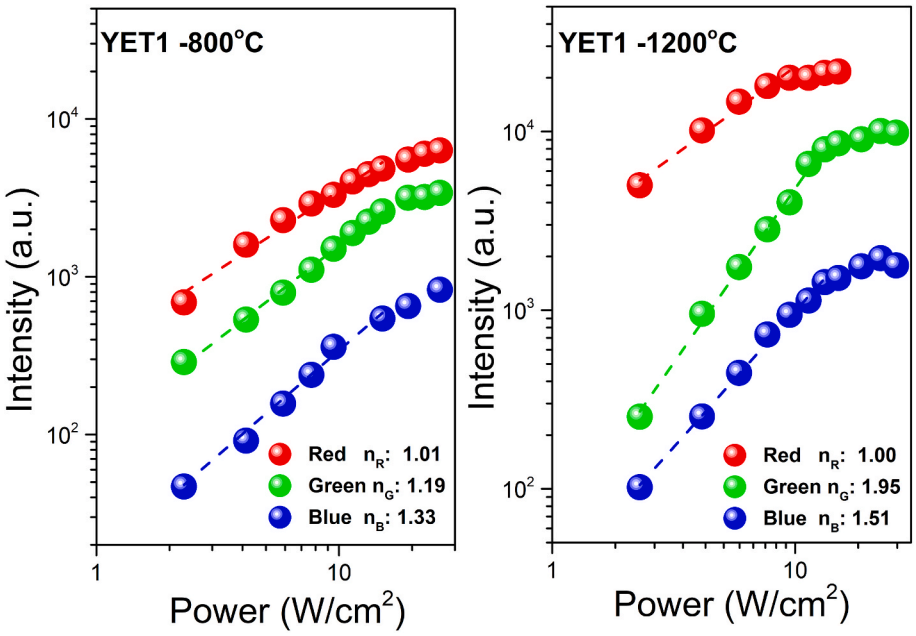

Fig. 6. Logarithmic plots of UC-emissions vs. laser excitation power for nanophosphors.

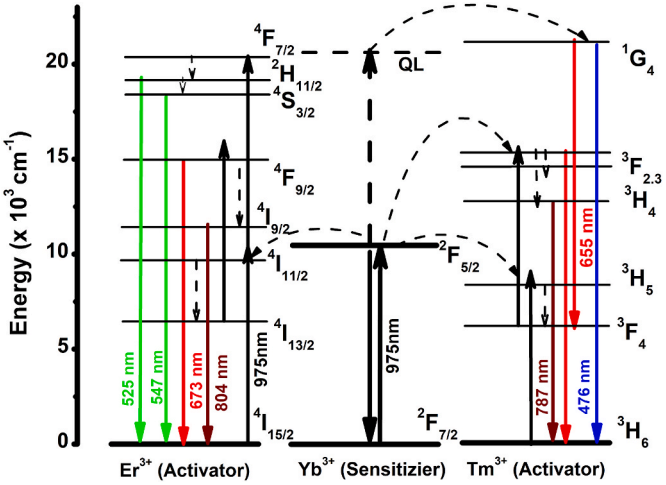

Fig. 7. Possible energy transfers between the Yb^{3+}, Er^{3+}, and Tm^{3+} ions in the energy-level diagram for the GGG nanocrystals.

To explain the possibility of energy transfers in nanophosphors, the number (n) of photons contributing to the absorption is found from the slope of the log-log plot of intensity versus power, shown in Fig. 6. The number of photons involved in the absorption process is based on two-photon transition processes for the blue, green, and red emissions.

3.4. Energy transfer processes

Fig. 7 shows the energy level diagram of Yb^{3+}, Er^{3+}, and Tm^{3+} ions in the GGG nanocrystals to explain possible energy transfer mechanisms such as ground state absorption (GSA), excited-state absorption (ESA), energy transfer (ET), and nonradiative relaxation (NRR).

The transfer of energy from the Yb^{3+} ions to the Tm^{3+} and Er^{3+} ions may moderately occur to fill those upper excited levels due to energy mismatch between the Er^{3+}/Tm^{3+} ions and Yb^{3+} ions in GGG nanocrystals. As indicated in Fig. 7, the following points can be pointed out for the energy transfer mechanism [35,36];

In the GGG system, Er^{3+} ions at the ground $^4I_{15/2}$ state are firstly populated to the $^4I_{11/2}$ excited state by ground-state absorption (GSA) via 975 nm laser excitation. Then the $^4I_{13/2}$ and $^4F_{7/2}$ levels can be populated by the NRR and energy transfer mechanisms, respectively. The population of $^4F_{7/2}$ level can be increased by the excited state absorption (ESA) of Er^{3+} ions and/or by the following energy transfer (ET): $^4I_{11/2}$ (Er^{3+}) + $^2F_{5/2}$ (Yb^{3+}) → $^4F_{7/2}$ (Er^{3+}) + $^2F_{7/2}$ (Yb^{3+}). The population of $^4S_{3/2}$ and $^2H_{11/2}$ levels is filled by the NRR from the $^4F_{7/2}$ level, which causes green emissions (525 and 547 nm). Transition of Er^{3+} ions from the $^4F_{9/2}$ level to the $^4I_{15/2}$ level causes red emission (673 nm), which occurred by the following energy transfer; $^4I_{13/2}$ (Er^{3+}) + $^2F_{5/2}$ (Yb^{3+}) → $^4F_{9/2}$ (Er^{3+}) + $^2F_{7/2}$ (Yb^{3+}). In addition, for 804 nm emission, the $^4I_{9/2}$ level can be filled from the $^4F_{9/2}$ level via NRR.

When we consider radiations from thulium ions, the $^1G_4$ excited energy level can be filled by energy transfer from the ground state Yb^{3+} ions via three-photon processes. However, it is seen that the number of photons absorbed for blue light obtained from the logarithmic intensity and power curves is two. As a result of the Yb^{3+} ion-pair interaction, two NIR (975 nm) photons are absorbed so that the Yb^{3+} ion pair can fill the

Table 2
The CIE-1931 (x; y) coordinates, CCT, and CRI values of the nanocrystals under 4.14 W/cm² laser excitation power density.

Nanophosphors	Annealing Temperature (°C)	CIE-1931 (x, y)	CCT (K)	CRI
YET1	800	(0.3555; 0.4094)	4856	67
YET2	800	(0.3095; 0.3772)	6364	85
YET3	800	(0.3060; 0.3661)	6571	89
YET1	1000	(0.4478; 0.4569)	3215	24
YET2	1000	(0.4186; 0.3641)	2979	25
YET3	**1000**	**(0.3244; 0.3297)**	**5891**	**70**
YET1	1200	(0.4245; 0.4780)	3715	34
YET2	1200	(0.4129; 0.4455)	3733	34
YET3	1200	(0.3597; 0.4160)	4764	61

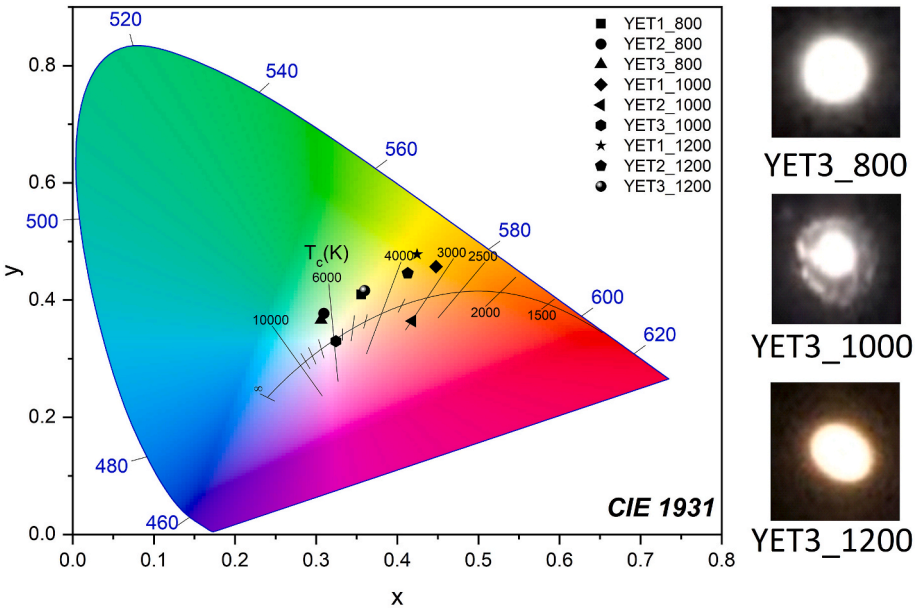

Fig. 8. CIE-1931 coordinates and emission photographs of YET:GGG nanophosphors with respect to different Tm^{3+} doping content and annealing temperature.

Table 3
Summary of Yb^{3+}/Er^{3+}/Tm^{3+} doped up-conversion nanophosphors (UCNPs) for single-component white light-emitting phosphors.

Phosphors	λ_{exc} (nm)	Power density P(W/cm^2) or Power (W)	Chromaticity coordinates (x, y)	Method	UC Band region	Ref
$Gd_3Ga_5O_{12}$	975 nm	4.14 W/cm^2 0.5 W	(0.3244, 0.3297)	Solgel Pechini method	Blue-Green-Red-NIR	This work
$Gd_3Ga_5O_{12}$	974.5 nm	16.3 W/cm^2 30.5 W/cm^2	(0.37, 0.42) (0.35, 0.41)	Propellant combustion Synthesis method	Blue-Green-Red	[28]
Y_2O_3	980 nm	34.87 W/cm^2	(0.32, 0.34)	Combustion method	Violet- Blue-Green-Red	[35]
$GdPO_4$	980 nm	3 W	(0.33, 0.38)	Solvothermal method	Blue-Green-Red	[36]
$Lu_3Ga_5O_{12}$	980 nm	3.4 W/cm^2	(0.27, 0.33)	Solgel method	Blue-Green-Red-NIR	[29]
CaF_2	980 nm	20 W/cm^2 32 W/cm^2	(0.337, 0.352) (0.310, 0.340)	Hydrothermal method	Violet-Blue-Green-Red	[37]
Gd_2O_3	980 nm	20 W/cm^2	(0.335, 0.336)	Wet-chemical method	Blue-Green-Red	[38]
KY_3F_{10}	980 nm	10.5 W/cm^2	(0.306, 0.363)	Hydrothermal method	Blue-Green-Red-NIR	[39]
$Gd_4O_3F_6$	980 nm	300 W/cm^2	(0.33, 0.34)	Coprecipitation method	Blue-Green-Red-NIR	[40]
α-TeO_2 β-TeO_2	980 nm	36.4 W/cm^2	(0.34, 0.33) (0.32, 0.33)	Hydrothermal method	Blue-Green-Red	[41]
$CaTiO_3$	976 nm	20 W/cm^2	(0.341, 0.335)	Solgel method	Blue-Green-Red	[42]
LaOF	980 nm	10 W/cm^2	(0.331, 0.368)	Modified Solgel Pechini method	Blue-Green-Red	[43]
Y_2O_3	975 nm	830 W/cm^2	(0.2910, 0.3831)	Thermal Decomposition method	Blue-Green-Red	[44]
SrF2	974 nm	4 × 10^5 W	(0.308, 0.332)	Co-precipitation method	Blue-Green-Red	[45]
Y_2SiO_5	950 nm	1.5 W	(0.334, 0.332)	Sol-gel method	Blue-Green-Red	[46]
$NaYF_4$	980 nm	7 W	(~0.33,~0.30)	Thermal Decomposition method	Blue-Green-Red	[47]
TiO_2	980 nm	2 × 10^3 W	(0.3175, 0.3382)	Sol-gel method	Blue-Green-Red	[34]
$Y_2Si_2O_7$	975 nm	352 W/cm^2	(0.3370,0.3303) (0.3063,0.3172)	Sol-gel method	Blue-Green-Red-NIR	[4]

so-called quasi-level (QL). Next, a cooperative sensitization process can populate the $^1G_4$ energy level of neighboring Tm^{3+} ions. Then the red (656 nm) and blue emissions (476 nm) occur by the relaxation of Tm^{3+} ions from the $^1G_4$ level to the $^3F_4$ and $^3H_6$ levels, respectively. In addition, the $^3F_{2,3}$ excited level is populated by two subsequent energy transfer processes from Yb^{3+} to Tm^{3+}: In the first, $^3H_5$ energy level is populated by the energy transfer (ET): $^3H_6$ (Tm^{3+}) + $^2F_{5/2}$ (Yb^{3+}) → $^3H_5$ (Tm^{3+}) +$^2F_{7/2}$ (Yb^{3+}). Then the population of $^3H_5$ decreases by the nonradiative energy transfer from the $^3H_5$ level to the $^3F_4$ level. In the second, The energy transfer from (ET): $^3F_4$ (Tm^{3+}) + $^2F_{5/2}$ (Yb^{3+}) → $^3F_{2,3}$ (Tm^{3+}) +$^2F_{7/2}$(Yb^{3+}) increases the population of the $^3F_{2,3}$ excited level to generate the red emission (656 nm). Then the $^3F_{2,3}$ level decays nonradiatively to the $^3H_4$ excited level to generate the infrared emission at 787 nm.

3.5. Color chromaticity properties

The CIE-1931 (x; y) coordinates, color temperature (CCT), and color rendering index (CRI) values of the nanopowders under 4.14 W/cm^2 excitation power density are shown in Table 2 and drawn in Fig. 8 for comparison. Changing the Tm^{3+} ion concentration affects the quality of the color coordinates, and as the Tm^{3+} concentration increases, the CCT and CRI values of its emissions increase. The CCT and CRI values of the nanopowders annealed at 800 °C vary between 4856 K and 6571 K and 67–89, respectively. The CIE-1931 color quality coordinates of $Gd_3Ga_5O_{12}$:2%Yb^{3+}/1%Er^{3+}/1.5%Tm^{3+} nanopowders annealed at

1000 °C fall well within the white zone (x = 0.3244, y = 0.3297). These results indicate that the single-component GGG nanophosphors can be suitable for solid-state lighting. We have also summarized $Yb^{3+}/Er^{3+}/Tm^{3+}$ tridoped up-conversion nanophosphors (UCNPs) for single-component white-emitting phosphors in literature (Table 3).

4. Conclusion

Triply doped gadolinium gallium garnet nanocrystals were synthesized using the Solgel Pechini method with different heat-treated and various $Yb^{3+}/Er^{3+}/Tm^{3+}$dopant ratios. The bright white up-conversion emission was obtained under the 975 nm laser excitation. Color chromaticity coordinates were shifted regularly with the pumping densities, the annealing temperatures, and the Tm^{3+} concentrations. Upon the 4.14 W/cm^2 laser excitation power density, bright white light is achieved in the $Gd_3Ga_5O_{12}$:2%Yb^{3+}/1%Er^{3+}/1.5%Tm^{3+} nanocrystals, and the calculated CIE color coordinates of (0.3244, 0.3297) fall well within the white zone. GGG could be considered an efficient host material under infrared excitation. GGG-based white upconverting phosphors may have potential applications in lighting technology, multicolor fluorescent labels, and plant curvation.

CRediT authorship contribution statement

Hümeyra Örücü: Conceptualization, Investigation, Visualization, Writing – original draft, Writing – review & editing. **Sevcan Tabanli:** Investigation, Visualization. **Murat Erdem:** Investigation, Visualization, Writing – review & editing. **Yavuz Öztürk:** Resources, Investigation. **Gönül Eryürek:** Resources, Supervision.

Declaration of competing interest

The authors declare that they have no known competing financial interests or personal relationships that could have appeared to influence the work reported in this paper.

Acknowledgments

This work was supported by project number 14-FEN-027 from Ege University Scientific Research Projects Coordination Department.

References

[1] M. Shang, C. Li, J. Lin, How to produce white light in a single-phase host? Chem. Soc. Rev. 43 (2014) 1372–1386, https://doi.org/10.1039/c3cs60314h.
[2] K. Zhang, L. Tong, Y. Ma, J. Wang, Z. Xia, Y. Han, Modulated up-conversion luminescence and low-temperature sensing of $Gd_3Ga_5O_{12}$:Yb^{3+}/Er^{3+} by incorporation of Fe^{3+} ions, J. Alloys Compd. 781 (2019) 467–472, https://doi.org/10.1016/j.jallcom.2018.12.147.
[3] R. Priya, O.P. Pandey, S.J. Dhoble, Review on the synthesis, structural and photophysical properties of Gd_2O_3 phosphors for various luminescent applications, Opt Laser. Technol. 135 (2021), 106663, https://doi.org/10.1016/j.optlastec.2020.106663.
[4] M. Erdem, S. Tabanli, G. Eryurek, R. Samur, B. Di Bartolo, Crystalline phase effect on the up-conversion processes and white emission of $Yb^{3+}/Er^{3+}/Tm^{3+}$:$Y_2Si_2O_7$ nanocrystals, Dalton Trans. 48 (2019) 6464–6472, https://doi.org/10.1039/c9dt00956f.
[5] G.B. Nair, V.B. Pawade, S.J. Dhoble, White light-emitting novel nanophosphors for LED applications, in: Nanomaterials for Green Energy, Elsevier Inc., 2018, pp. 411–431, https://doi.org/10.1016/B978-0-12-813731-4.00013-8.
[6] A. Tiwari, S.J. Dhoble, Tunable lanthanide/transition metal ion-doped novel phosphors for possible application in w-LEDs: a review, Luminescence 35 (2020) 4–33, https://doi.org/10.1002/bio.3712.
[7] V.V. Atuchin, N.F. Beisel, E.N. Galashov, E.M. Mandrik, M.S. Molokeev, A. P. Yelisseyev, A.A. Yusuf, Z. Xia, Pressure-stimulated synthesis and luminescence properties of Microcrystalline $(Lu,Y)_3Al_5O_{12}$:Ce^{3+} garnet phosphors, ACS Appl. Mater. Interfaces 7 (2015) 26235–26243, https://doi.org/10.1021/acsami.5b08411.
[8] K.S. Kumar, C. Lou, Y. Xie, L. Hu, A. Gowri Manohari, D. Xiao, H. Ye, L. Tang, D. Pribat, Energy transfer in co- and tri-doped $Y_3Al_5O_{12}$ phosphors, J. Rare Earths 35 (2017) 775–782, https://doi.org/10.1016/S1002-0721(17)60975-X.
[9] I. Levchuk, A. Osvet, C.J. Brabec, M. Batentschuk, A. Shakhno, T. Zorenko, Y. Zorenko, Micro-powder $Ca_3Sc_2Si_3O_{12}$:Ce silicate garnets as efficient light converters for WLEDs, Opt. Mater. 107 (2020), https://doi.org/10.1016/j.optmat.2020.109978, 109978.
[10] T. Gao, J. Tian, Y. Liu, R. Liu, W. Zhuang, Garnet phosphors for white-light-emitting diodes: modification and calculation, Dalton Trans. 50 (2021) 3769–3781, https://doi.org/10.1039/d0dt04368k.
[11] R. Praveena, K. Balasubrahmanyam, L. Jyothi, G. Venkataiah, C. Basavapoornima, C.K. Jayasankar, White light generation from Dy^{3+}-doped yttrium aluminium gallium mixed garnet nano-powders, J. Lumin. 170 (2016) 262–270, https://doi.org/10.1016/j.jlumin.2015.10.012.
[12] A. Speghini, F. Piccinelli, M. Bettinelli, Synthesis, characterization and luminescence spectroscopy of oxide nanopowders activated with trivalent lanthanide ions: the garnet family, Opt. Mater. 33 (2011) 247–257, https://doi.org/10.1016/j.optmat.2010.10.039.
[13] T.J. Garino, J.A. Voigt, E.D. Spoerke, D.L. Moore, S.J. Lockwood, J.T. Gibson, P. Yang, J.T. Gibson, C.C. Phifer, Development of a Manufacturing Capability for Production of Ceramic Laser Materials, n.d., 2007. Sandia National Laboratories Report
[14] S. Jia, Q. Liu, J. Li, J. Li, X. Zhou, S. Xiang, Q. Wu, Refractive indices of shock-induced polymorphic $Gd_3Ga_5O_{12}$ single crystals, J. Appl. Phys. 126 (2019), 205902, https://doi.org/10.1063/1.5116159.
[15] F. Vetrone, J.C. Boyer, J.A. Capobianco, A. Speghini, M. Bettinelli, Luminescence spectroscopy and near-infrared to visible upconversion of nanocrystalline $Gd_3Ga_5O_{12}$:Er^{3+}, J. Phys. Chem. B 107 (2003) 10747–10752, https://doi.org/10.1021/jp030434r.
[16] M. Pang, J. Lin, Growth and optical properties of nanocrystalline $Gd_3Ga_5O_{12}$: Ln (Ln = Eu^{3+}, Tb^{3+}, Er^{3+}) powders and thin films via Pechini sol-gel process, J. Cryst. Growth 284 (2005) 262–269, https://doi.org/10.1016/j.jcrysgro.2005.07.007.
[17] X. Tian, X. Zhang, Y. Li, P. Yang, Synthesis and spectral properties of Nd^{3+}: $Gd_3Ga_5O_{12}$ nanopowder for transparent laser ceramics, J. Rare Earths 24 (2006) 443–446, https://doi.org/10.1016/S1002-0721(06)60140-3.
[18] M. Daldosso, D. Falcomer, A. Speghini, M. Bettinelli, S. Enzo, B. Lasio, S. Polizzi, Synthesis, structural investigation and luminescence spectroscopy of nanocrystalline $Gd_3Ga_5O_{12}$ doped with lanthanide ions, J. Alloys Compd. 451 (2008) 553–556, https://doi.org/10.1016/j.jallcom.2007.04.194.
[19] S.K. Singh, D.G. Lee, S.S. Yi, K. Jang, D.S. Shin, J.H. Jeong, Probing dual-mode emission of Eu3+ in garnet phosphor, J. Appl. Phys. 113 (2013), 173504, https://doi.org/10.1063/1.4803053.
[20] M. Rathaiah, A.D. Lozano-Gorrín, P. Babu, C.K. Jayasankar, V. Lavín, V. Venkatramu, Efficient Nd^{3+} sensitized Yb^{3+} emission and infrared-to-visible energy conversion in gallium nano-garnets, RSC Adv. 6 (2016) 78669–78677, https://doi.org/10.1039/c6ra13729f.
[21] J.C. Boyer, F. Vetrone, J.A. Capobianco, A. Speghini, M. Bettinelli, Yb^{3+} ion as a sensitizer for the upconversion luminescence in nanocrystalline $Gd_3Ga_5O_{12}$:Ho^{3+}, Chem. Phys. Lett. 390 (2004) 403–407, https://doi.org/10.1016/j.cplett.2004.04.047.
[22] F. Pandozzi, F. Vetrone, J.C. Boyer, R. Naccache, J.A. Capobianco, A. Speghini, M. Bettinelli, A spectroscopic analysis of blue and ultraviolet upconverted emissions from $Gd_3Ga_5O_{12}$:Tm^{3+},Yb^{3+} nanocrystals, J. Phys. Chem. B 109 (2005) 17400–17405, https://doi.org/10.1021/jp052192w.
[23] R. Naccache, F. Vetrone, A. Speghini, M. Bettinelli, J.A. Capobianco, Cross-relaxation and upconversion processes in Pr^{3+} singly doped and Pr^{3+}/Yb^{3+} codoped nanocrystalline $Gd_3Ga_5O_{12}$: the sensitizer/activator relationship, J. Phys. Chem. C 112 (2008) 7750–7756, https://doi.org/10.1021/jp711494d.
[24] M. Erdem, H. Örücü, S.B. Cantürk, G. Eryürek, Upconversion Yb^{3+}/Er^{3+}: gadolinium gallium garnet nanocrystals for white-light emission and optical thermometry, ACS Appl. Nano Mater. 4 (2021) 7162–7171, https://doi.org/10.1021/acsanm.1c01140.
[25] C. Sun, W. Lü, F. Yang, C. Tu, Tunable red-green-blue multicolor luminescence in $Yb^{3+}/Tm^{3+}/Ho^{3+}$:$Gd_3Ga_5O_{12}$ nano-crystals, J. Alloys Compd. 512 (2012) 160–164, https://doi.org/10.1016/j.jallcom.2011.09.056.
[26] J. Sun, G. Sun, Y. Sun, L. Han, Luminescence properties and energy transfer investigations of tri-doped Sr_3AlO_4F:Ce^{3+},Tb^{3+},Yb^{3+} phosphors, Opt. Mater. 36 (2014) 1097–1100, https://doi.org/10.1016/j.optmat.2014.01.023.
[27] L. Tong, K. Saito, Q. Guo, H. Zhou, T. Fan, D. Zhang, Defect induced visible-light-activated near-infrared emissions in $Gd_{3xyz}Yb_xBi_yEr_zGa_5O_12$, J. Appl. Phys. 122 (2017) 173103. https://doi.org/10.1063/1.5001974.
[28] C. Sun, W. Lü, X. Ma, T. Cao, J. Li, Z. Zhu, Z. You, Y. Wang, C. Tu, White up-conversion luminescent property in Re^{3+}:$Gd_3Ga_5O_{12}$ nanocrystals, J. Nanosci. Nanotechnol. 10 (2010) 6527–6533, https://doi.org/10.1166/jnn.2010.2620.
[29] V. Mahalingam, F. Mangiarini, F. Vetrone, V. Venkatramu, M. Bettinelli, A. Speghini, J.A. Capobianco, Bright white upconversion emission from $Tm^{3+}/Yb^{3+}/Er^{3+}$-doped $Lu_3Ga_5O_{12}$ nanocrystals, J. Phys. Chem. C 112 (2008) 17745–17749.
[30] R.D. Shannon, Revised effective ionic radii and systematic studies of interatomic distances in halides and chalcogenides, Acta Crystallogr. A32 (1976) 751–767.
[31] P. Guo, G. Li, F. Zhao, F. Liao, S. Tian, X. Jing, New phases of R_3GaO_6 (R=Rare earth elements) and their luminescent properties, J. Electrochem. Soc. 150 (2003) H201, https://doi.org/10.1149/1.1595666.
[32] P. Scherrer, Bestimmung der Grosse und der inneren Struktur von Kolloidterilchen mittels Rontgestrahlen, Nachrichten von Der Gesellschaft Der Wissenschaften Zu Göttingen, Math. Klasse (1918) 98–100.
[33] J. Li, J. Sun, J. Liu, X. Li, J. Zhang, Y. Tian, S. Fu, L. Cheng, H. Zhong, H. Xia, B. Chen, Pumping-route-dependent concentration quenching and temperature effect of green up- and down-conversion luminescence in Er^{3+}/Yb^{3+} co-doped $Gd_2(WO_4)_3$ phosphors, Mater. Res. Bull. 48 (2013) 2159–2165, https://doi.org/10.1016/j.materresbull.2013.02.009.

[34] J. Dong, Y. Li, W. Zheng, R. Wang, Y. Xu, Lower power-dependent upconversion multicolor tunable properties in TiO_2:Yb^{3+}/Er^{3+}/(Tm^{3+}), Ceram. Int. 45 (2019) 432–438, https://doi.org/10.1016/j.ceramint.2018.09.184.

[35] V.K. Rai, R. Dey, K. Kumar, White upconversion emission in Y_2O_3:Er^{3+}-Tm^{3+}-Yb^{3+}phosphor, Mater. Res. Bull. 48 (2013) 2232–2236, https://doi.org/10.1016/j.materresbull.2013.02.064.

[36] M.A. Hassairi, A. Garrido Hernández, M. Dammak, D. Zambon, G. Chadeyron, R. Mahiou, Tuning white upconversion emission in GdPO4:Er/Yb/Tm phosphors, J. Lumin. 203 (2018) 707–713, https://doi.org/10.1016/j.jlumin.2018.07.024.

[37] C. Cao, W. Qin, J. Zhang, Y. Wang, G. Wang, G. Wei, P. Zhu, L. Wang, L. Jin, Up-conversion white light of Tm^{3+}/Er^{3+}/Yb^{3+} tri-doped CaF_2 phosphors, Opt Commun. 281 (2008) 1716–1719, https://doi.org/10.1016/j.optcom.2007.11.045.

[38] K. Zheng, D. Zhang, D. Zhao, N. Liu, F. Shi, W. Qin, Bright white upconversion emission from Yb^{3+}, Er^{3+}, and Tm^{3+}-codoped Gd_2O_3 nanotubes, Phys. Chem. Chem. Phys. 12 (2010) 7620–7625, https://doi.org/10.1039/b922230h.

[39] T. Pang, W. Cao, M. Xing, X. Luo, X. Yang, Design and achieving mechanism of upconversion white emission based on Yb^{3+}/Tm^{3+}/Er^{3+} tri-doped KY_3F_{10} nanocrystals, Opt. Mater. 33 (2011) 485–489, https://doi.org/10.1016/j.optmat.2010.10.037.

[40] T. Passuello, F. Piccinelli, M. Pedroni, M. Bettinelli, F. Mangiarini, R. Naccache, F. Vetrone, J.A. Capobianco, A. Speghini, White light upconversion of nanocrystalline Er/Tm/Yb doped tetragonal $Gd_4O_3F_6$, Opt. Mater. 33 (2011) 643–646, https://doi.org/10.1016/j.optmat.2010.11.017.

[41] H. Hu, Y. Bai, Upconversion white luminescence of TeO_2:Tm^{3+}/Er^{3+}/Yb^{3+} nanoparticles, J. Alloys Compd. 527 (2012) 25–29, https://doi.org/10.1016/j.jallcom.2012.02.129.

[42] X. Chen, Y. Li, F. Kong, L. Li, Q. Sun, F. Wang, Red, green, blue and bright white upconversion luminescence of $CaTiO_3$: Er^{3+}/Tm^{3+}/Yb^{3+} nanocrystals, J. Alloys Compd. 541 (2012) 505–509, https://doi.org/10.1016/j.jallcom.2012.07.008.

[43] K. Zheng, Y. Liu, Z. Liu, Z. Chen, W. Qin, Color control and white upconversion luminescence of LaOF:Ln^{3+} (Ln = Yb, Er, Tm) nanocrystals prepared by the sol-gel Pechini method, Dalton Trans. 42 (2013) 5159–5166, https://doi.org/10.1039/c3dt32721c.

[44] S. Tabanli, G. Eryurek, Upconversion luminescence properties of Y_2O_3: Yb^{3+}/Er^{3+}/Tm^{3+} nanocrystal doped PMMA nanocomposites, J. Non-Cryst. Solids 505 (2019) 43–51, https://doi.org/10.1016/j.jnoncrysol.2018.10.041.

[45] Y.A. Rozhnova, A.A. Luginina, V.V. Voronov, R.P. Ermakov, S.V. Kuznetsov, A. V. Ryabova, D.V. Pominova, V.V. Arbenina, V.V. Osiko, P.P. Fedorov, White light luminophores based on Yb^{3+}/Er^{3+}/Tm^{3+}-coactivated strontium fluoride powders, Mater. Chem. Phys. 148 (2014) 201–207, https://doi.org/10.1016/j.matchemphys.2014.07.032.

[46] M. Erdem, O. Erguzel, M.K. Ekmekci, H. Orucu, H. Cinkaya, S. Genc, A. Mergen, G. Eryurek, B. Di Bartolo, Bright white up-conversion emission from sol–gel derived Yb^{3+}/Er^{3+}/Tm^{3+}: Y_2SiO_5 nanocrystalline powders, Ceram. Int. 41 (2015) 12805–12810, https://doi.org/10.1016/j.ceramint.2015.06.116.

[47] Z. Yu, X. Li, X. Wang, Y. Yang, White up-conversion efficiency of Yb^{3+}/Er^{3+}/Tm^{3+} co-doped β-NaYF4 nano-crystals, J. Lumin. 207 (2019) 48–52, https://doi.org/10.1016/j.jlumin.2018.10.121.